applied sciences

MDPI

Article

Closed Form Constraint Equations Used to Express Frictionless Slip of Multibody Systems Attached to Finite Elements—Application to a Contact between a Double Pendulum and a Beam

Krzysztof Lipinski

Faculty of Mechanical Engineering and Ship Technology, Gdansk University of Technology, ul. Narutowicza 11/12, 80-233 Gdansk, Poland; klipinsk@pg.edu.pl

Abstract: This paper focuses on the numerical modeling of the dynamics of mechanical systems. Robots that can inspect high-voltage lines inspired this research. Their control systems must anticipate potential grab positions appropriately. We intend to formulate equations dedicated to the numerical description of the robot/cable contact. The investigated problem is not straightforward, since parts of the modeled systems are numerically inhomogeneous. They consist of multibody and finite element components. These components interact with each other only through frictionless point contact. We limit the present investigation to the mathematical modeling of these frictionless point connections. According to the model-adopted assumption, the location of the contact point is invariant in the multibody structure, but it is variable in the finite elements part. Unlike the classically used models (i.e., spring/damper models of elastic contacts), we focus on constraint equations. We present and discuss their details in this paper. Following the presence of the constraint equations, their associated Lagrange multipliers appear in the dynamics equations of the two sub-models. The main feature/result of the presently proposed method is the closed form of the coordinate-portioning formulae, proposed in this paper, employed to eliminate the dependent coordinates and the constraint-associated Lagrange multipliers. To verify the applicability of the proposed elimination methodology, we test its use in a dedicated numerical example. During the test, we limit the investigation to a frictionless connection between a double pendulum and a beam. The results confirm that the proposed methodology allows us to model the investigated frictionless contact. We shall underline a vital property, that the proposed elimination method is universal, and thus one can easily extend/modify the above methodology to operate with other multibody/finite element contacts.

Keywords: mechanical engineering; multibody dynamics; finite elements; constraints; frictionless sliding

Citation: Lipinski, K. Closed Form Constraint Equations Used to Express Frictionless Slip of Multibody Systems Attached to Finite Elements—Application to a Contact between a Double Pendulum and a Beam. *Appl. Sci.* **2023**, *13*, 3681. https://doi.org/10.3390/app13063681

Academic Editor: Alessandro Ruggiero

Received: 25 January 2023
Revised: 2 March 2023
Accepted: 7 March 2023
Published: 14 March 2023

1. Introduction

The investigated coincidence of a multibody subsystem and a finite elements subsystem is a typical technical situation, and one can find an extensive list of examples in the scientific literature. Pantograph/catenary systems used to supply trains with their electrical currents are the typical examples presented in [1–4]. Flexible multibody systems [5–7], bio-mechanical models [8,9], vehicle wheel/ground contacts [10], or vehicle wheel/rail contacts [11] are other typical examples.

The target point of the conducted research is bio-inspired mobile robots, with the aim of reconstructing in them the natural behaviour and mobility of gibbons. The principal mode of their locomotion (brachiation) consists of swinging from branch to branch for distances of up to 15 m at speeds as fast as 50 km/h. We should point out several constructions proposed in the technical literature [12–15] dedicated to the so-called brachiation robots. Because of the similarities of their investigated aspects, we can categorize them as a branch of walking

robots. Research focusing on the dynamics of brachiation robots involves multitasking. Firstly, we need to investigate uncertain nonlinear time-varying systems. Its number of degrees of freedom varies during its motion. Secondly, unilateral constraints are present, and impact forces can appear in the system. Thirdly, at selected stages of locomotion, the examined systems are kinematically or dynamically overactuated. As a result, many different intelligent and robust control schemes are proposed in the technical literature to control this non-typical class of brachiation robots. One can use these brachiation robots to detect faults in voltage transmission lines. One can use them to perform any needed tasks during natural disasters or catastrophes. They can document any incident from various angles. These robots can inspect and clean cables (e.g., shake off icing) at a height that is dangerous for humans.

As discussed above, brachiation is not a straightforward method of motion. A particularly complex issue is its control. If one intends to grab a cable, the robot has to move its arm and its temporally free gripper to a spatial position, which is identical to the localization of the grab cable. Since brachiating is not a slow-speed kinetostatic process, it is necessary to determine/anticipate the appropriate moment of grip activation for each subsequent cadence of the movement. With the elastic deformable vibrating nature of the deformations, the actual position of the cable is not the a priori known constant of the system, especially since the other-hand interaction is not the neutral quantity in the investigation. If present, this dynamics interaction (i.e., the one appearing at the contact point between the robot and the beam) can significantly modify the system dynamics. Since it is a bilateral interaction, the robot dynamics can affect the beam dynamics, and any beam dynamics may change the robot dynamics. Let us focus on rational and effective methods of controlling this type of robot. Three techniques are predominant. The first one is a visual control. We may use it if the systems possess sufficient optical detectors. Secondly, one can experimentally identify the system dynamics (and its time mutability). Several methods and techniques may help us with experimental identifications. The adaptive multiscale morphological filter [16] and the time-frequency ridge estimation [17] are examples. Finally, one can model the dynamics of the subparts of the investigated system. The present paper limits its attention to details regarding the last of the proposed control techniques. This is primarily because the presently assumed application of the robot is to brachiate in unknown, previously unexplored environments. Further, breaks in its locomotion (unavoidable during identification) are not allowed from the point of view of the dynamics.

We are unable to present all the above aspects in a single paper. We focus on one of them, i.e., a sliding (frictionless) contact between the robot and the cable. A quick overview of the bibliographic positions [1–3,6–9] allows us to verbalize a conclusion that if frictionless point contacts connect the multibody and finite elements subparts, the most popular and the most classic contact modeling method is the lumped-mass spring or the lumped spring/damper element introduced as a connecting component. As a straightforward consequence of this method, numerical integrations of these subparts are quasi-independent, i.e., the algorithms can treat the dynamics of both subparts independently and calculate the shared interaction force outside of the two models. To correlate these simulations, at each step of the calculation, the algorithms estimate the relative penetration for the contact, i.e., they compare the position of the selected tip of the interacting body of the multibody structure with the location of the point at the contact line of its deformable counterpart. Then they use the penetration to estimate the contact force, and they use sets of a priori assumed elasticity and damping parameters for these estimations. The algorithms add the above-calculated contact forces to the dynamics of both subparts, i.e., both parts treat it as an external force. The proposed method is attractive, mainly due to its simplicity. It has an inspirational physical interpretation referring to a spring or a damping/spring element. From a mathematical point of view, however, the above approach is a penalty method. Let us point out that the penalty method is a commonly accepted mathematical tool, extensively used in many areas, e.g., in investigations of constrained systems and optimization techniques. The attractiveness of the recalled fusion of the physical and math-

ematical interpretations is validated additionally by the fact that the relative displacement (together with its derivatives) is the only parameter used to evaluate the intercorrelating parameter that constrains the dynamics descriptions of the two abovementioned subsystems. The above description refers to its canonical version. Modified versions of the algorithm were proposed in the literature, also. Paper [10] referred to selected parameters of relative penetration, but these were employed to evaluate strains, and the last of these affected the finite elements of the elastic counterpart of the contact. Antunes et al. [11] adopted the Hertzian model of contact force (with some additional damping hysteresis) to evaluate the surface-orthogonal component of the contact force. In [6], an extensive list of penalty functions was recalled from the literature and tested numerically. Skrinjar et al. proposed an extension of the list in [18]. In [19], Atanasovska extended the set of bodies used to model the contact. An additional fictional deformable body was introduced in the space partly/temporarily released by the physical contacting bodies and coupled with them by a set of time-varying stiffness and damping elements.

The constraint/multipliers method is also used/known in the broadly understood field of contact analyses. One can find bibliographic examples of its application in [4,5,20–26]. As pointed out in [20], the multipliers method defeats most of the typical ill-conditioning problems (critical in many cases of penalty methods). Moreover, by applying the multipliers method, the geometrical conditions of the contacts are fulfilled precisely [20], and stability of the system is achieved by fulfilling the energy preservation and energy decay statements for the elastic bodies [5]. However, we should point out that the presence of Lagrange's multipliers enforces an additional increase in the size of the matrices, and supplementary numerical operations are necessary to evaluate the actual values of the multipliers. If one focuses on the multibody systems and numerical calculations of systems extended with the multipliers, and if one investigates the details of the last operations, two algorithms are dominant. These are the elimination and augmentation philosophies. In the bibliography of dynamics of the constrained multibody/finite elements systems, the augmentation philosophy is predominant [4,5,20–22]. The elimination philosophy is rather less common [23–26].

Cavalieri et al. proposed to compile these two methods (modified Rockefeller-Lagrangian strategy) in [20]. Following opinions presented in [20], one should interpret the method as a variety of the well-known idea of an augmented Lagrangian method. Of course, both methods (i.e., the augmented Lagrangian and penalty methods) require penalty parameters. However, their roles are less critical in the augmented Lagrangian method [20], since they are used only to correct the convergence of the constraints. As the main benefit of this modified strategy, the Lagrange multipliers may be estimated less accurately, for example, with simplified algorithms.

The present paper recalls the idea of using constraint equations, and we dedicate this idea to the analyses of frictionless point contacts. We set its principal focus on two independent aspects: equations used to model the geometrical constraints of the connection (I), and appropriate coordinate partitioning and proper multipliers elimination (II). Selected elements of the first aspect have been considered in the literature in the past [5,20–22,24–26]. The second aspect has not been explored intensively, especially for multibody/finite element contacts [23–26]. Thus, potential fields of numerical examinations and simplifications are accessible in the above context. We intend to fill the research gap observed in the literature. The main feature/result of the presently proposed method is the closed form of the coordinate-portioning formulae employed to eliminate the dependent coordinates and the constraint-associated Lagrange multipliers, as presented in this paper.

We divided the paper into nine sections. Section 2 presents the fundamentals of the multibody formalisms used. It illustrates the principal properties of the elements used and the fundamental equations. Then, Section 3 details the background of the finite elements method employed in this paper. Again, the focus is set on the predominant properties of these elements and the properties of the resulting mathematical model. In the Section 4, the constraint equations proposed in this paper are presented and discussed. This section

focuses on the methods used to evaluate the Jacobian as well as the velocity level and the acceleration level constraints. This section also presents the coordinate partitioning proposed in this paper, mainly the consequences of the linearized form of the dynamics equations of the finite elements system. Section 5 presents the physical model used to test the proposed method of contact modeling. Section 6 details the dedicated numerical models of the continuous parts, associated with this paper. Section 7 details the matrices of the investigated multibody structure. Section 8 presents the obtained results of the numerical calculations. Finally, Section 9 presents conclusions and perspectives.

2. Employed Methodology of Kinematics and Dynamics of Three-like Multibody Systems

This paper recalls the classic definition of multibody structures interpreted as systems composed of interconnected non-deformable bodies. An additional assumption states that relative displacements can only occur at joints. All joints are single-degree-of-freedom massless elements. One can assume displacements of the joint as the generalized coordinates of the system. The joint displacements are significant in magnitude (especially at the rotational joints). Following [26–28], one can employ the classic concept of the kinematical chain (Figure 1a).

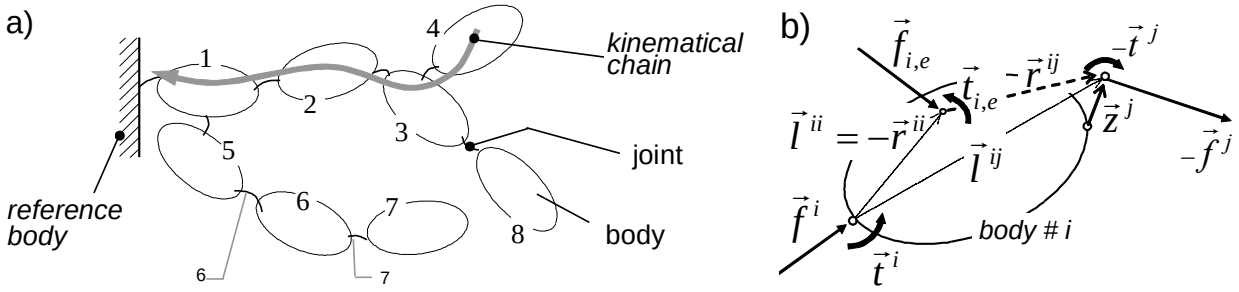

Figure 1. Elements of multibody structure: joints, bodies, and numbering (**a**); geometrical distances at *body i* and interactions acting on the body (**b**).

Suppose body #*i* is the generic body of the system; $\overline{x}^i$, is the vector of the absolute position of its centre of mass, Ci (with respect to the origin of the base-fixed frame); and $\boldsymbol{T^i}$ is the absolute orientation matrix of the body-fixed coordinate system (with respect to the base-fixed frame). One can write the vector and the matrix as the sum and product of the relative subparts.

$$\overline{x}^i = \sum_{j:j\le i} \left(p^k \cdot \overline{a}^k + \overline{d}^{ji} \right) = \sum_{j:j\le i} \overline{l}^{ji}; \boldsymbol{T}^i = \prod_{j:j\le i} \boldsymbol{R}^j, \tag{1}$$

Next, their time derivatives allow us to write the velocity and acceleration formulae. This leads to [26–28]:

$$\dot{\overline{x}}^i = \sum_{k:k\le i} \left(\dot{p}^k \cdot \overline{a}^k + \overline{\omega}^k \times \overline{l}^{ki} \right); \tag{2a}$$

$$\overline{\omega}^i = \sum_{k:k\le i} \dot{\phi}^k \cdot \overline{e}^k, \tag{2b}$$

$$\ddot{\overline{x}}^i = \sum_{k:k\le i} \left(\ddot{p}^k \cdot \overline{a}^k + \dot{\overline{\omega}}^k \times \overline{l}^{ki} + 2\dot{p}^k \cdot \overline{\omega}^k \times \overline{a}^k + \overline{\omega}^k \times \left(\overline{\omega}^k \times \overline{l}^{ki} \right) \right); \tag{2c}$$

$$\dot{\overline{\omega}}^i = \sum_{k:k\le i} \left(\ddot{\phi}^k \cdot \overline{e}^k + \dot{\phi}^k \cdot \overline{\omega}^k \times \overline{e}^k \right), \tag{2d}$$

where $\overline{a}^j$ is the unit vector of direction of translation line at joint #*j* (unit vector collinear to the line of the translation; it is the zero vector for rotational joints); $\overline{e}^j$ is the unit vector of direction of rotation at joint #*j* (collinear to the rotation axis; it is the zero vector when one examines translational joints); p^j is the magnitude of translations at the joint #*j*; and φ^j is the value of the rotation angle at this joint #*j*.

To obtain the dynamics equations, one should cut all joints of the system and introduce the joint's interactions to replace the cut connections (Figure 1b). Then, Newton/Euler dynamics equations are written for each of the free-body diagrams of all bodies of the system [26–28]:

$$m^i \cdot \ddot{\overline{x}}^i = \overline{f}^i + \overline{f}^{i,e} - \sum_{j \in i^+} \overline{f}^j ; \tag{3a}$$

$$\overline{\omega}^i \times (\overline{\overline{I}}^i \cdot \overline{\omega}^i) + \overline{\overline{I}}^i \cdot \dot{\overline{\omega}}^i = \overline{t}^{i,e} + \overline{r}^{ii} \times \overline{f}^i + \overline{t}^i - \sum_{j \in i^+} \overline{t}^j - \sum_{j \in i^+} \overline{r}^{ij} \times \overline{f}^j, \tag{3b}$$

where m^i is a mass of body #i; $\overline{\overline{I}}^i$ is its tensor of moments of inertia (calculated about the centre of mass of the body #i); $\overline{f}^i$, $\overline{t}^i$ are the joint force and torque, respectively, at the cut joint #i that act on body #i, $\overline{f}^{i,e}$ is a net external force that acts at the mass centre of body #i; and $\overline{t}^{i,e}$ is the net external torque that acts on body #i.

The dynamics Equation (3a,b) are complemented with the velocity formulae (2a,b) and the acceleration formulae (2c,d). Next, one can eliminate the successors' forces and the successors' torques from (3a,b). We propose to use a backward evaluation. This starts from the dynamics equations written for the leaf bodies (successor-free bodies). Then, there are investigated bodies with a completed list of the dynamics equations of all their successors. For all of them, one can replace the successors' forces and torques with formulae obtained in the previous steps. Next, we project each successor-free equation on the unit vector of mobility of the principal/fixing joint of the body (we project the force at joint #i on the vector $\overline{a}^i$, and the torque on the vector $\overline{e}^i$, respectively). Finally, we factor out the joint accelerations from the terms, viz., we collect all of the components in front of the accelerations as elements of the mass matrix. One can write the resulting formulae in the standard form [26–28],

$$\boldsymbol{M}_b(\boldsymbol{q}_b) \cdot \ddot{\boldsymbol{q}}_b + \boldsymbol{F}_b(\dot{\boldsymbol{q}}_b, \boldsymbol{q}_b) = \boldsymbol{Q}(\dot{\boldsymbol{q}}_b, \boldsymbol{q}_b, \boldsymbol{f}_e, \boldsymbol{t}_e, t), \tag{4}$$

where $\boldsymbol{M}_b$ is the square mass matrix of the multibody part; $\boldsymbol{q}_b$ is the column matrix of its generalized coordinates (the joint displacements of the reference tree structure); $\boldsymbol{F}_b$ is the column matrix of the velocity-based inertial effects; $\boldsymbol{Q}_b$ is the column matrix of the generalized forces of the system; $\boldsymbol{f}_e$, $\boldsymbol{t}_e$ are external forces and torques, respectively; and t is time.

3. Kinematics and Dynamics of the Elastic Part

The investigated elastic subpart belongs (is fixed) to the motionless base of the system. Therefore, we can omit the kinematics formulae resulting from its transport motion. To model the elastic subpart, we use the classic finite elements technique. A finite set of nodal points is selected. Their displacements are the assumed system's generalized coordinates. Since we investigate the elastic beams instead of the nodal points, nodal cross sections are permitted, and thus, each of the nodes has its six degrees of freedom mobility with respect to the base (i.e., translational and rotational degrees). Of course, in particular analyses, the investigated number of nodal degrees could be lower (e.g., for planar beam elements, two degrees of freedom are sufficient, i.e., the vertical and rotational degrees are allowed; the longitudinal degrees are the locked ones) (Figure 2).

A motionless global coordinate system fixed to the reference body/base is the collective reference system of the subpart. However, if one investigates any intermediate stage of deriving the dynamics equations, one also can introduce a set of local systems. They are associated with each finite element and can simplify the estimation of components of the used vectors. Even if one dedicates them to the deformable elements, the local systems remain stationary (fixed to the motionless reference coordinate system but fitted to the initial positions of the undeformed finite elements). By convention, a hat $\hat{}$ is used at the top of the parameter to denote coordinates measured in the local system. When the particular limited cases of motion of nodes of a beam element are considered (Figure 2),

the only non-locked coordinates are the vertical displacement of the nodes (along the y2 axis) and its rotations (made about the y3 axis). In addition, two nodes are sufficient to express the displacements of a beam element. Let one number the nodes as node #*i* and node #*j*. Further, if we focus on loads of the subpart, formally, they can be attached to any particular particle of the detail, but when we investigate the finite elements, their attachment points are limited solely to the nodes of the system. With these assumptions, matrices of coordinates of this element and matrices of the forces are [24–26,29–31],

$$\widehat{\boldsymbol{q}}_{be} = col\left(\widehat{q}_{i2}, \widehat{q}_{i6}, \widehat{q}_{j2}, \widehat{q}_{j6}\right); \widehat{\boldsymbol{P}}_{be} = col\left(\widehat{P}_{i2}, \widehat{P}_{i6}, \widehat{P}_{j2}, \widehat{P}_{j6}\right) \tag{5}$$

where $\widehat{q}_{i2}$, $\widehat{q}_{j2}$ are the translational motion of the nodes along the y_2 axis (Figure 3); $\widehat{q}_{i6}$, $\widehat{q}_{j6}$ are the magnitudes of the rotations of the nodes about y_3 (Figure 2); $\widehat{P}_{i2}$, $\widehat{P}_{j2}$ are the forces at the nodes of the finite element, set as collinear to y_2; and $\widehat{P}_{i6}$, $\widehat{P}_{j6}$ are the torques at the nodes of the finite element, set as collinear to y_3.

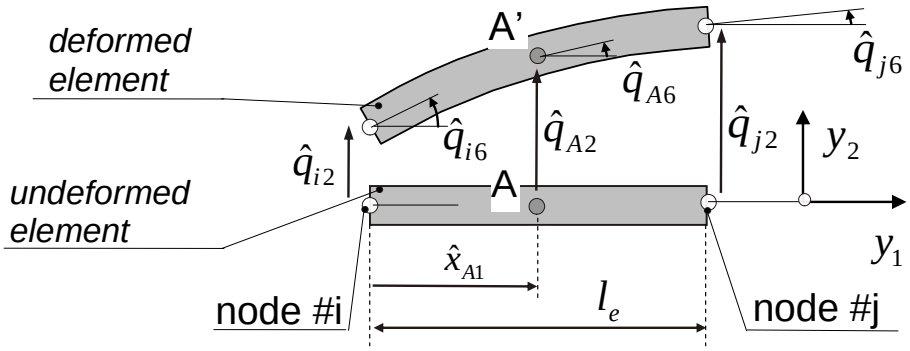

Figure 2. Selected displacements of investigated planar beam element (displacements of the nodes and of the generic point *A*).

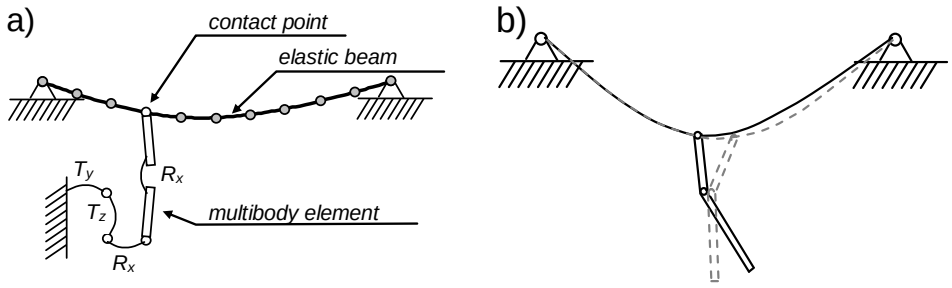

Figure 3. The investigated system: a sketch of its hybrid finite elements/multibody structure (**a**); selected poses of the beam and the pendulum (**b**).

The constitutive assumption of the finite elements method states that each continuous property and continuous characteristic of the element is a linear function of values of this property, measured at the nodes. Factors of these linear functions depend on the relative position of the investigated point with respect to the localization of its associated reference nodes. To minimize the simplification errors of the above approximation, the size of the elements should be small. According to this approximation, displacements of the not-nodal generic point A, denoted here as $\hat{\boldsymbol{\Delta}}^A \equiv \hat{\boldsymbol{\Delta}}$, can be expressed as [24–26,29–31],

$$\hat{\boldsymbol{\Delta}} = \hat{\boldsymbol{N}}_{\boldsymbol{e}} \cdot \hat{\boldsymbol{\Delta}}_{\boldsymbol{e}} = \hat{\boldsymbol{N}}_{\boldsymbol{e}} \cdot \hat{\boldsymbol{q}}_{\boldsymbol{e}}, \tag{6}$$

where $\hat{\boldsymbol{\Delta}}_{\boldsymbol{e}} = col(\hat{\Delta}_{i2}, \hat{\Delta}_{i6}, \hat{\Delta}_{j2}, \hat{\Delta}_{j6})$ is the vector of the displacements measured at the nodes of the element; $\hat{\boldsymbol{\Delta}} = col(\hat{\Delta}_2, \hat{\Delta}_6)$ is the vector of displacements of the generic point; and

$\hat{\boldsymbol{N}}_{\boldsymbol{e}} = \left[\hat{N}_{e1}, \hat{N}_{e2}, \hat{N}_{e3}, \ldots, \hat{N}_{ew}\right]$ is the matrix of the shape functions, associated with the assumed type of the finite element.

Because the shape functions are time independent, therefore the velocity of the generic point (time derivative of its displacement) is [24–26,29–31],

$$\hat{v} = \dot{\hat{\Delta}} = \hat{N}_e \cdot \dot{\hat{q}}_e, \tag{7}$$

and linear deformations, $\hat{\varepsilon}$, of the generic point are [24–26,29–31]:

$$\hat{\varepsilon} = \hat{B}_l \cdot \hat{q}_e; \tag{8a}$$

$$\hat{B}_l = \Gamma_l \cdot \hat{N}_e = \begin{bmatrix} \frac{\partial}{\partial x_1} & 0 & 0 & \frac{\partial}{\partial x_2} & 0 & \frac{\partial}{\partial x_3} \\ 0 & \frac{\partial}{\partial x_2} & 0 & \frac{\partial}{\partial x_1} & \frac{\partial}{\partial x_3} & 0 \\ 0 & 0 & \frac{\partial}{\partial x_3} & 0 & \frac{\partial}{\partial x_2} & \frac{\partial}{\partial x_1} \end{bmatrix}^T \cdot \hat{N}_e, \tag{8b}$$

where $\hat{B}_l$ is a matrix that correlates deformations of the generic point with the displacements of the nodes; and Γ_l is the linear operator of differentiations (one can take its general form from many positions, e.g. [30,31]).

The stress/strain relation of the element depends significantly on the stress/strain configuration. When one assumes the planar state of the stresses, the formula is [24–26,29,30]:

$$\hat{\sigma} = \hat{D}_e \cdot \hat{\varepsilon}; \tag{9a}$$

$$\hat{D}_e = \frac{E_e}{1 - v^2} \begin{bmatrix} 1 & v & 0 \\ & 1 & 0 \\ sym. & & 0.5 \cdot (1 - v) \end{bmatrix}, \tag{9b}$$

where E_e is Young's modulus of elasticity; and v is Poisson's ratio of the substance of the beam.

Recalling (7)–(9) in the kinetic energy formula, one can write the total kinetic energy, *Ee*, of the element, as well as the total energy of its deformation, *Ve*, as [24–26,29–31]:

$$E_e = \frac{1}{2} \int_{m_e} \hat{v}^T \cdot \hat{v} \cdot dm; \tag{10b}$$

$$V_e = \frac{1}{2} \int_{V_e} \hat{\varepsilon}^T \cdot \hat{\sigma} \cdot dV, \tag{10b}$$

and rewritten to [24–26,29–31]:

$$E_e = \frac{1}{2} \dot{\hat{q}}_e^T \cdot \hat{M}_e \cdot \dot{\hat{q}}_e; \tag{11a}$$

$$\hat{M}_e = \frac{1}{2} \rho \cdot \int_{x_e} \int_{y_e} \int_{z_e} \hat{N}_e^T \cdot \hat{N}_e \cdot dx \cdot dy \cdot dz; \tag{11b}$$

$$V_e = \frac{1}{2} \hat{q}_e^T \cdot \hat{K}_e \cdot \hat{q}_e; \tag{12a}$$

$$\hat{K}_e = \frac{1}{2} \int_{x_e} \int_{y_e} \int_{z_e} \hat{B}_l^T \cdot \hat{D}_e \cdot \hat{B}_l \cdot dx \cdot dy \cdot dz, \tag{12b}$$

where the obtained matrices $\hat{M}_e$ and $\hat{K}_e$ are the mass matrix and the elasticity/stiffness matrix, respectively, of the element expressed in the local coordinate system.

We can omit the subsequent step of classic development now since if we focus on the presently investigated case, the local systems are collinear to the global system, and therefore rotational transformations are unnecessary. Accordingly, the local coordinates are identical to their absolute complements.

If one intends to obtain the global vector of the displacements, $\boldsymbol{q}_c^*$, and the global vector of loads, $\boldsymbol{P}_c^*$, all the elements' matrices of displacements and loads should be grouped and written as:

$$\boldsymbol{q}_c^* = col(\boldsymbol{q}_i); \tag{13a}$$

$$\boldsymbol{P}_c^* = col(\boldsymbol{P}_i), \tag{13b}$$

where $\boldsymbol{q}_i$ is the vector of displacements of the ith node; and $\boldsymbol{P}_i$ is the vector of loads of the ith node.

Furthermore, one can write the global matrices for the shape functions, masses, and elasticity components. With a correct allocation of blocs of the local matrices:

$$Neqe = [\ NiNj\ ]ij[qiqj]ij\ ; \quad Aeqe = [AiiAijAjiAjj]ij[qiqj]ij\ , \tag{14}$$

one can write the global matrices as [24–26,29–31]:

$$\boldsymbol{N}_e^* \cdot \boldsymbol{q}_c^* = \begin{bmatrix} 0 & \boldsymbol{N_i} & 0 & \boldsymbol{N_j} & 0 \\ \dots & i & \dots & j & \dots \end{bmatrix} \cdot \begin{bmatrix} \boldsymbol{q}_{1-i} \\ \boldsymbol{q_i} \\ \boldsymbol{q}_{i-j} \\ \boldsymbol{q_j} \\ \boldsymbol{q}_{j-n_e} \end{bmatrix} \begin{matrix} \vdots \\ i \\ \vdots \\ j \\ \vdots \end{matrix} ; \quad \boldsymbol{A}_e^* \cdot \boldsymbol{q}_c^* = \begin{bmatrix} 0 & 0 & 0 & 0 & 0 \\ 0 & \boldsymbol{A_{ii}} & 0 & \boldsymbol{A_{ij}} & 0 \\ 0 & 0 & 0 & 0 & 0 \\ 0 & \boldsymbol{A_{ji}} & 0 & \boldsymbol{A_{jj}} & 0 \\ 0 & 0 & 0 & 0 & 0 \\ \dots & i & \dots & j & \dots \end{bmatrix} \cdot \begin{bmatrix} \boldsymbol{q}_{1-i} \\ \boldsymbol{q_i} \\ \boldsymbol{q}_{i-j} \\ \boldsymbol{q_j} \\ \boldsymbol{q}_{j-n_e} \end{bmatrix} \begin{matrix} \vdots \\ i \\ \vdots \\ j \\ \vdots \end{matrix} . \tag{15}$$

Then, thanks to the cumulative property of the kinetic and potential energy, the global matrices of the subpart are obtained as sums of all the matrices of elements [24–26,29–31]:

$$\boldsymbol{M}_c^* = \sum_{e=1}^{n_e} \boldsymbol{M}_e^*; \tag{16a}$$

$$\boldsymbol{K}_c^* = \sum_{e=1}^{n_e} \boldsymbol{K}_e^*, \tag{16b}$$

where n_e is a number of the finite elements considered in the system.

Finally, one can eliminate rows and columns that correspond to the locked nodes (constrained points of the analysed detail), and the final form of the dynamics equations is [24–26,29–31]:

$$\boldsymbol{M}_c \cdot \ddot{\boldsymbol{q}}_c + \boldsymbol{K}_c \cdot \boldsymbol{q}_c = \boldsymbol{P}_c; \tag{17a}$$

$$\boldsymbol{\Delta} = \boldsymbol{N}_e^c \cdot \boldsymbol{q}_c, \tag{17b}$$

or, when one assumes some damping properties,

$$\boldsymbol{M}_c \cdot \ddot{\boldsymbol{q}}_c + \boldsymbol{C}_c \cdot \dot{\boldsymbol{q}}_c + \boldsymbol{K}_c \cdot \boldsymbol{q}_c = \boldsymbol{P}_c; \tag{18a}$$

$$\boldsymbol{\Delta} = \boldsymbol{N}_e^c \cdot \boldsymbol{q}_c. \tag{18b}$$

4. Constraints Formulae and Dynamics of the Constrained System

If focusing on the presently investigated case, longitudinal slip is possible, and it is the free one, i.e., only the vertical degree of freedom is locked. Accordingly, the vertical component of displacement of the beam contact point (obtained in the motionless global coordinate system fixed to the reference body) is the same as the vertical component of the vertex of the multibody. This leads to:

$$\Phi^s = r_{p2}^{cb} - r_{p2}^{b} = 0 \tag{19}$$

where r_{p2}^{cb} is the vertical component of the point at the elastic body; and r_{p2}^{b} is the vertical component of the vertex of the rigid body.

Since slip is allowed, if one investigates the position of the contact point at the elastic body, its vertical component depends on the coordinates of the investigated finite element (via the vertical vector component of the displacement formula). However, this also depends on the multibody coordinates (by its longitudinal position along the axis of the beam). Following the idea of Equation (6), the Jacobian of the constraint can be written as [26]:

$$\boldsymbol{\Phi}(\boldsymbol{q_b}, \boldsymbol{q_c}, \varsigma) = \boldsymbol{N}(\varsigma)\cdot\boldsymbol{q}_c - p_n(\boldsymbol{q}_b) = 0 \tag{20}$$

where $p_n(\boldsymbol{q_b})$ is the vertical position of the contact point calculated as position of a point of the multibody subpart; and $\boldsymbol{q_b}, \boldsymbol{q_c}, \varsigma$ are the pointed-out functions of time.

Since we express the contact imposed between the multibody subpart and the finite elements subpart as a constraint equation, we need to add the Lagrange multipliers to the dynamics equations. As a result, the previously obtained differential equations of dynamics are converted to their differentially algebraic form [26]:

$$\begin{gathered}\boldsymbol{M}_b(\boldsymbol{q}_b)\cdot\ddot{\boldsymbol{q}}_b + \boldsymbol{F}_b\left(\dot{\boldsymbol{q}}_b, \boldsymbol{q}_b\right) + \boldsymbol{J}_b^T(\boldsymbol{q}_b)\cdot\lambda = \boldsymbol{Q}_b\left(\dot{\boldsymbol{q}}_b, \boldsymbol{q}_b, \boldsymbol{f_e}, \boldsymbol{t_e}, t\right) ; \\ \boldsymbol{M}_c\cdot\ddot{\boldsymbol{q}}_c + \boldsymbol{D}_c\cdot\dot{\boldsymbol{q}}_c + \boldsymbol{K}_c\cdot\boldsymbol{q}_c + \boldsymbol{J}_c^T\cdot\lambda = \boldsymbol{P}_c ; \\ \boldsymbol{\Phi}(\boldsymbol{q}_c, \boldsymbol{q}_b) = \boldsymbol{N}\cdot\boldsymbol{q}_c - p_n(\boldsymbol{q}_b) = 0 \;\; ; \;\; \boldsymbol{J}_b = \frac{\partial}{\partial \boldsymbol{q_b}}\boldsymbol{\Phi} \;\; ; \;\; \boldsymbol{J}_c = \frac{\partial}{\partial \boldsymbol{q_c}}\boldsymbol{\Phi} ,\end{gathered} \tag{21}$$

The joined set of the coordinates (composed of multibody coordinates and nodal coordinates) is partitioned into independent (understood as selectable) and dependent (understood as computable) coordinates. To eliminate velocities and accelerations of the dependent coordinates, derivatives of the constraint equations are necessary. We propose to write them as [24–26]:

$$\begin{gathered}\boldsymbol{N}\cdot\dot{\boldsymbol{q}}_c + \dot{\xi}\cdot\boldsymbol{N}_\xi\cdot\boldsymbol{q}_c - \boldsymbol{J}\cdot\dot{\boldsymbol{q}}_b = 0 \;\; ; \\ \boldsymbol{N}\cdot\ddot{\boldsymbol{q}}_c + \ddot{\xi}\cdot\boldsymbol{N}_\xi\cdot\boldsymbol{q}_c + 2\dot{\xi}\cdot\boldsymbol{N}_\xi\cdot\dot{\boldsymbol{q}}_c + \dot{\xi}^2\cdot\boldsymbol{N}_{\xi\xi}\cdot\boldsymbol{q}_c - \left(\boldsymbol{J}\cdot\dot{\boldsymbol{q}}_b\right)_q\cdot\dot{\boldsymbol{q}}_b - \boldsymbol{J}\cdot\ddot{\boldsymbol{q}}_b = 0 \;\; :\end{gathered} \tag{22}$$

where:

$$\begin{gathered}\boldsymbol{J} = \frac{\partial}{\partial \boldsymbol{q_b}}p_n = -\boldsymbol{J}_b \; ; \;\; \dot{\xi} = v_t(\dot{\boldsymbol{q}}_b, \boldsymbol{q}_b)/l \; ; \; \ddot{\xi} = a_t(\ddot{\boldsymbol{q}}_b, \dot{\boldsymbol{q}}_b, \boldsymbol{q}_b)/l \; ; \\ \boldsymbol{N}_\xi = \frac{\partial}{\partial \xi}\boldsymbol{N} \;\; ; \;\; \boldsymbol{N}_{\xi\xi} = \frac{\partial^2}{\partial \xi^2}\boldsymbol{N} \;\; ; \;\; \left(\boldsymbol{J}\cdot\dot{\boldsymbol{q}}_b\right)_q = \frac{\partial}{\partial \boldsymbol{q_b}}\left(\boldsymbol{J}\cdot\dot{\boldsymbol{q}}_b\right) \;\; ; \;\; \boldsymbol{J}_c = \boldsymbol{N} ;\end{gathered} \tag{23}$$

and where v_t is the horizontal speed of the contact point; and a_t is the horizontal acceleration of the point.

Of course, the investigated horizontal position of the contact point depends on the kinematics of the multibody part, and thus one can write the horizontal speed and acceleration as [24–26]:

$$\begin{gathered}\dot{\xi} = (1/l)\cdot\boldsymbol{J}_t\cdot\dot{\boldsymbol{q}}_b \;\; ; \;\; \ddot{\xi} = (1/l)\cdot\boldsymbol{J}_t\cdot\ddot{\boldsymbol{q}}_b + \gamma_t \;\; ; \;\; \boldsymbol{N}\cdot\dot{\boldsymbol{q}}_c + \boldsymbol{J}_R\cdot\dot{\boldsymbol{q}}_b = 0 \;\; ; \\ \boldsymbol{N}\cdot\ddot{\boldsymbol{q}}_c + \boldsymbol{J}_R\cdot\ddot{\boldsymbol{q}}_b + 2\dot{\xi}\cdot\boldsymbol{N}_\xi\cdot\dot{\boldsymbol{q}}_c + \dot{\xi}^2\cdot\boldsymbol{N}_{\xi\xi}\cdot\boldsymbol{q}_c + (1/l)\,\boldsymbol{N}_\xi\cdot\boldsymbol{q}_c\cdot\gamma_T - \gamma = 0 \;\; : \\ \boldsymbol{J}_t = \frac{\partial}{\partial \boldsymbol{q_b}}p_t \; ; \; \boldsymbol{J}_R = (1/l)\cdot\boldsymbol{N}_\xi\cdot\boldsymbol{q}_c\cdot\boldsymbol{J}_t - \boldsymbol{J} \; ; \; \gamma_t = \left(\boldsymbol{J}_t\cdot\dot{\boldsymbol{q}}_b\right)_q\cdot\dot{\boldsymbol{q}}_b \; ; \; \gamma = \left(\boldsymbol{J}\cdot\dot{\boldsymbol{q}}_b\right)_q\cdot\dot{\boldsymbol{q}}_b ,\end{gathered} \tag{24}$$

where $p_t(\boldsymbol{qb})$ is the horizontal position of the contact point calculated as the position of a generic point of the multibody subpart; and $\boldsymbol{J}_t$ is the matrix of partial derivatives of the horizontal position of this generic point.

As pointed out in the introduction, we employ the elimination philosophy in this paper to solve the differentially algebraic form of the dynamics equations. Therefore, we shall eliminate the dependent coordinates and the Lagrange multipliers. The elimination philosophy is a classical tool of multibody analyses. One can find the main steps of the philosophy in [32]. In the present paper, we examine certain reformulations based on the linearity of the dynamics of the finite elements subpart. In the presently used version of the algorithm, we uniquely operate with the multibody coordinates, $\boldsymbol{q}_b$, to be partitioned into dependent, $\boldsymbol{v}$, and independent, $\boldsymbol{u}$, coordinates. All coordinates, $\boldsymbol{q}_c$, of the continuous finite

elements subpart are assumed as independent. As a result, we can write the dynamics equation of the multibody subpart as:

$$\boldsymbol{M}_{buu}\cdot\ddot{\boldsymbol{u}} + \boldsymbol{M}_{buv}\cdot\ddot{\boldsymbol{v}} + \boldsymbol{F}_{bu} + \boldsymbol{J}_{bu}^{T}\cdot\boldsymbol{\lambda} = \boldsymbol{Q}_{bu}\,; \tag{25a}$$

$$\boldsymbol{M}_{bvu}\cdot\ddot{\boldsymbol{u}} + \boldsymbol{M}_{bvv}\cdot\ddot{\boldsymbol{v}} + \boldsymbol{F}_{bv} + \boldsymbol{J}_{bv}^{T}\cdot\boldsymbol{\lambda} = \boldsymbol{Q}_{bv}\,, \tag{25b}$$

and we can calculate the multipliers $\boldsymbol{\lambda}$ from (25a). This leads to

$$\boldsymbol{\lambda} = -\boldsymbol{J}_{bu}^{-T}\cdot\boldsymbol{M}_{buu}\cdot\ddot{\boldsymbol{u}} - \boldsymbol{J}_{bu}^{-T}\cdot\boldsymbol{M}_{buv}\cdot\ddot{\boldsymbol{v}} - \boldsymbol{J}_{bu}^{-T}\cdot\boldsymbol{F}_{bu} + \boldsymbol{J}_{bu}^{-T}\cdot\boldsymbol{Q}_{bu}. \tag{26}$$

Further, the constraint equations (at their acceleration level) are partitioned. Accordingly, we can write the dependent accelerations as

$$\begin{gathered}\ddot{\boldsymbol{v}} = -\boldsymbol{J}_{Rv}^{-1}\cdot\boldsymbol{N}\cdot\ddot{\boldsymbol{q}}_c - \boldsymbol{J}_{Rv}^{-1}\cdot\boldsymbol{J}_{Ru}\cdot\ddot{\boldsymbol{u}} + \\ -\boldsymbol{J}_{Rv}^{-1}\cdot\left(2\dot{\xi}\cdot\boldsymbol{N}_{\xi}\cdot\dot{\boldsymbol{q}}_c + \dot{\xi}^{2}\cdot\boldsymbol{N}_{\xi\xi}\cdot\boldsymbol{q}_c + (1/l)\cdot\boldsymbol{N}_{\xi}\cdot\boldsymbol{q}_c\cdot\gamma_T - \gamma\right).\end{gathered} \tag{27}$$

We eliminate the obtained multipliers and accelerations from the dynamic equations of the multibody subsystem. Then, one can apply the standard form used in multibody dynamics to express the dynamics of the resulting system,

$$\boldsymbol{M}_{11}\cdot\ddot{\boldsymbol{u}} + \boldsymbol{M}_{12}\cdot\ddot{\boldsymbol{q}}_c + \boldsymbol{F}_1 = \boldsymbol{Q}_1, \tag{28}$$

where:

$$\begin{gathered}\boldsymbol{M}_{11} = \boldsymbol{M}_{bvu} - \boldsymbol{J}_{bv}^{T}\cdot\boldsymbol{J}_{bu}^{-T}\cdot\boldsymbol{M}_{buu} - \boldsymbol{M}_{bvv}\cdot\boldsymbol{J}_{Rv}^{-1}\cdot\boldsymbol{J}_{Ru} + \boldsymbol{J}_{bv}^{T}\cdot\boldsymbol{J}_{bu}^{-T}\cdot\boldsymbol{M}_{buv}\cdot\boldsymbol{J}_{Rv}^{-1}\cdot\boldsymbol{J}_{Ru}\,; \\ \boldsymbol{M}_{12} = -\boldsymbol{M}_{bvv}\cdot\boldsymbol{J}_{Rv}^{-1}\cdot\boldsymbol{N} + \boldsymbol{J}_{bv}^{T}\cdot\boldsymbol{J}_{bu}^{-T}\cdot\boldsymbol{M}_{buv}\cdot\boldsymbol{J}_{Rv}^{-1}\cdot\boldsymbol{N}\,; \\ \boldsymbol{Q}_1 = \boldsymbol{Q}_{bv} - \boldsymbol{J}_{bv}^{T}\cdot\boldsymbol{J}_{bu}^{-T}\cdot\boldsymbol{Q}_{bu}\,; \\ \boldsymbol{F}_1 = \boldsymbol{F}_{bv} - \boldsymbol{J}_{bv}^{T}\cdot\boldsymbol{J}_{bu}^{-T}\cdot\boldsymbol{F}_{bu} + \\ -\left(\boldsymbol{M}_{bvv} - \boldsymbol{J}_{bv}^{T}\cdot\boldsymbol{J}_{bu}^{-T}\cdot\boldsymbol{M}_{buv}\right)\cdot\boldsymbol{J}_{Rv}^{-1}\cdot\left(2\dot{\xi}\cdot\boldsymbol{N}_{\xi}\cdot\dot{\boldsymbol{q}}_c + \dot{\xi}^{2}\cdot\boldsymbol{N}_{\xi\xi}\cdot\boldsymbol{q}_c + (1/l)\cdot\boldsymbol{N}_{\xi}\cdot\boldsymbol{q}_c\cdot\gamma_T - \gamma\right).\end{gathered} \tag{29}$$

We shall also eliminate the obtained multipliers from the dynamic equation of the finite elements subpart. To deal with this, we shall initially exclude the dependent accelerations from the Lagrange terms (26). Therefore, we can write the final result of both eliminations in a hybrid finite elements/multibody form,

$$\boldsymbol{M}_{21}\cdot\ddot{\boldsymbol{u}} + \boldsymbol{M}_{22}\cdot\ddot{\boldsymbol{q}}_c + \boldsymbol{D}_2\cdot\dot{\boldsymbol{q}}_c + \boldsymbol{K}_2\cdot\boldsymbol{q}_c + \boldsymbol{F}_2 = \boldsymbol{P}_2 \tag{30}$$

where:

$$\begin{gathered}\boldsymbol{M}_{21} = -\boldsymbol{J}_{c}^{T}\cdot\boldsymbol{J}_{bu}^{-T}\cdot\boldsymbol{M}_{buu} + \boldsymbol{J}_{c}^{T}\cdot\boldsymbol{J}_{bu}^{-T}\cdot\boldsymbol{M}_{buv}\cdot\boldsymbol{J}_{Rv}^{-1}\cdot\boldsymbol{J}_{Ru}\,;\ \boldsymbol{M}_{21} = \boldsymbol{M}_c + \boldsymbol{J}_{c}^{T}\cdot\boldsymbol{J}_{bu}^{-T}\cdot\boldsymbol{M}_{buv}\cdot\boldsymbol{J}_{Rv}^{-1}\cdot\boldsymbol{N}\,; \\ \boldsymbol{D}_2 = \boldsymbol{D}_c + \boldsymbol{J}_{c}^{T}\cdot\boldsymbol{J}_{bu}^{-T}\cdot\boldsymbol{M}_{buv}\cdot\boldsymbol{J}_{Rv}^{-1}\cdot 2\dot{\xi}\cdot\boldsymbol{N}_{\xi}\ ;\ \boldsymbol{K}_2 = \boldsymbol{K}_c + \boldsymbol{J}_{c}^{T}\cdot\boldsymbol{J}_{bu}^{-T}\cdot\boldsymbol{M}_{buv}\cdot\boldsymbol{J}_{Rv}^{-1}\cdot\dot{\xi}^{2}\cdot\boldsymbol{N}_{\xi\xi}\,; \\ \boldsymbol{F}_2 = -\boldsymbol{J}_{c}^{T}\cdot\boldsymbol{J}_{bu}^{-T}\cdot\boldsymbol{F}_{bu} + \boldsymbol{J}_{c}^{T}\cdot\boldsymbol{J}_{bu}^{-T}\cdot\boldsymbol{M}_{buv}\cdot\boldsymbol{J}_{Rv}^{-1}\cdot\left((1/l)\cdot\boldsymbol{N}_{\xi}\cdot\boldsymbol{q}_c\cdot\gamma_T - \gamma\right)\ ; \\ \boldsymbol{P}_2 = \boldsymbol{P}_c - \boldsymbol{J}_{c}^{T}\cdot\boldsymbol{J}_{bu}^{-T}\cdot\boldsymbol{Q}_{bu}\,.\end{gathered} \tag{31}$$

5. Considered System

We numerically test the effectiveness of the introduced equations. The test-used exemplary model corresponds to a planar beam connected with a double pendulum that oscillates and slides on this beam (Figure 1a). Since we set the principal focus on the constraint equations, the beam is modeled with the use of 50 finite elements, only. The number of the used elements is low, but we have to remember that the high precision of modeling of the beam behaviour is not the critical point of the present investigation. In the prepared numerical model, both the abovementioned elements are introduced. We introduce the abovementioned constraint equations in the same form as we present them in the above

parts of the paper, as well as employing the above-presented method of coordinate partitioning and elimination. Finally, obtained dynamic equations are integrated numerically.

The investigated multibody system is planar and composed of four bodies. The bodies construct a single serial kinematical chain. If one starts counting from the reference body, the two first joints are translational, and the two last joints are rotational (each being a single degree of freedom). The first two bodies are fictitious massless elements. The first arm (body #3) is 1.5 m long. Its mass equals 20 kg, its mass centre is in the geometrical centre of its length, its moment of inertia is 2 kg·m^2 (with respect to the mass centre), and its inertia products equal zero. The second arm is 1 m long. Its mass equals 20 kg, its mass centre is in the geometrical centre of its length, the moment of inertia is 2 kg·m^2, and its inertia products equal zero. The beam's length equals 5 m, and 50 finite elements are used to model it (we intend to validate the behaviour of the numerical model; the detailed investigation of beam vibrations is not in the scope of the present tests). The surface of its cross sections equals 1.5×10^{-4} m^2. The beam's geometrical moment of inertia equals 2.81×10^{-9} m^4, and the density of its material is 7.86×10^3 kg/m^3. Its Young modulus equals 2.1×10^{11} Pa.

6. Details of Matrices of the Investigated Beam Elements

Let us be reminded that the present test is limited solely to planar beam elements (Figure 3). We use cubic functions as the shape functions used to model these elements (the cubic form is necessary to preserve the continuity of the deformations when focusing on contacts of the neighbour elements). Corresponding shape functions are [24–26,29–31],

$$\widehat{\boldsymbol{N}}_{\boldsymbol{e}}(\zeta) = \begin{bmatrix} \widehat{\boldsymbol{N}}_{2\boldsymbol{e}}(\zeta) \\ \widehat{\boldsymbol{N}}_{6\boldsymbol{e}}(\zeta) \end{bmatrix} = \begin{bmatrix} 2\zeta^3 - 3\zeta^2 + 1 & l_e(\zeta^3 - 2\zeta^2 + \zeta) & -2\zeta^3 + 3\zeta^2 & l_e(\zeta^3 - \zeta^2) \\ \frac{6(\zeta^2 - \zeta)}{l_e} & 3\zeta^2 - 4\zeta + 1 & \frac{6(-\zeta^2 + \zeta)}{l_e} & 3\zeta^2 - 2\zeta \end{bmatrix}, \quad (32)$$

where $\zeta = \widehat{x}_1 / l_e$ is the relative position of the considered cross section with respect to the initial/undeformed length of the element, l_e.

For consistency of the presentation, let us point out that we can use the first row of the matrix (32) to determine the vertical displacement of the central point of the cross section when the second one expresses the rotation of the section. Corresponding matrices of mass and elasticity are [24–26,29–31]:

$$\hat{\boldsymbol{M}}_{\boldsymbol{e}} = \frac{\rho_e \, A_e \, l_e}{420} \begin{bmatrix} 156 & 22l_e & 54 & -13l_e \\ & 4l_e^2 & 13l_e & -3l_e^2 \\ & & 156 & -22l_e \\ sym. & & & 4l_e^2 \end{bmatrix}, \quad \hat{\boldsymbol{K}}_{\boldsymbol{e}} = \frac{E_e \, J_e}{l_e^3} \begin{bmatrix} 12 & 6l_e & -12 & 6l_e \\ & 4l_e^2 & -6l_e & 2l_e^2 \\ & & 12 & -6l_e \\ sym. & & & 4l_e^2 \end{bmatrix}, \quad (33)$$

where A_e is an area of the beam's cross section (assumed as a constant one along the element); ρ_e is the volumetric mass density of the substance; and J_e is the area moment of inertia of the cross section.

7. Details of Matrices of the Investigated Multibody Structure

If one applies the abovementioned algorithm of multibody dynamics to the investigated multibody subpart (Figure 3a), one can obtain the following equations for elements of the matrices:

$$M_{14} = -l_z^4 \cdot m^4 \cdot c_{3p4}; \quad (34a)$$

$$M_{24} = -l_z^4 \cdot m^4 \cdot s_{3p4}; \quad (34b)$$

$$M_{34} = I^4 + l_z^4 \cdot m^4 \cdot \left(l_z^4 + d_z^4 \cdot c_4 \right); \quad (34c)$$

$$M_{44} = I^4 + l_z^4 \cdot l_z^4 \cdot m^4; \quad (34d)$$

$$M_{13} = -l_z^4 \cdot m^4 \cdot c_{3p4} - c_3 \cdot \left(d_z^4 \cdot m^4 + l_z^3 \cdot m^3 \right); \tag{34e}$$

$$M_{23} = -l_z^4 \cdot m^4 \cdot s_{3p4} - s_3 \cdot \left(d_z^4 \cdot m^4 + l_z^3 \cdot m^3 \right); \tag{34f}$$

$$M_{33} = I^4 + I^3 + l_z^4 \cdot m^4 \cdot \left(l_z^4 + d_z^4 \cdot c_4 \right) + d_z^4 \cdot m^4 \cdot \left(d_z^4 + l_z^4 \cdot c_4 \right) + l_z^3 \cdot l_z^3 \cdot m^3; \tag{34g}$$

$$M_{11} = M_{22} = m^3 + m^4 \tag{34h}$$

$$F_4 = \dot{q}_3 \cdot \dot{q}_3 \cdot d_z^4 \cdot l_z^4 \cdot m^4 \cdot s_4 + l_z^4 \cdot g \cdot m^4 \cdot s_{3p4}; \tag{34i}$$

$$F_3 = l_z^4 \cdot g \cdot m^4 \cdot s_{3p4} + g \cdot s_3 \cdot \left(d_z^4 \cdot m^4 + l_z^3 \cdot m^3 \right) - \dot{q}_4 \cdot \dot{q}_4 \cdot d_z^4 \cdot l_z^4 \cdot m^4 \cdot s_4 - 2 \cdot \dot{q}_3 \cdot \dot{q}_4 \cdot d_z^4 \cdot l_z^4 \cdot m^4 \cdot s_4; \tag{34j}$$

$$F_2 = -\dot{q}_3 \cdot \dot{q}_3 \cdot \left(l_z^4 \cdot m^4 \cdot c_{3p4} + c_3 \cdot \left(d_z^4 \cdot m^4 + l_z^3 \cdot m^3 \right) \right) - \dot{q}_4 \cdot l_z^4 \cdot m^4 \cdot c_{3p4} \cdot \left(2 \cdot \dot{q}_3 + \dot{q}_4 \right) - g \cdot \left(m^3 + m^4 \right); \tag{34k}$$

$$F_1 = \dot{q}_3 \cdot \dot{q}_3 \cdot \left(l_z^4 \cdot m^4 \cdot s_{3p4} + s_3 \cdot \left(d_z^4 \cdot m^4 + l_z^3 \cdot m^3 \right) \right) + \dot{q}_4 \cdot l_z^4 \cdot m^4 \cdot s_{3p4} \cdot \left(2 \cdot \dot{q}_3 + \dot{q}_4 \right); \tag{34l}$$

where $c_i = \cos(q_i)$; $s_i = \sin(q_i)$; $c_{3p4} = \cos(q_3 + q_4)$; $s_{3p4} = \sin(q_3 + q_4)$; d_z^4 is the length of the upper body of the pendulum; l_z^i is the vertical component of position of the mass centre of body #*i* with respect to the fixing point of joint #*i*; m^i is the mass of body #*i*; I^i is the moment of inertia of body #*i* with respect to its mass centre; and g is the gravity acceleration.

8. Obtained Results

To test the proposed equations, we wrote a numerical program in Matlab [33]. In the performed numerical test, all multibody joints are free of load (except for the pre-initial state of its equilibrium). At the pre-initial time instant, we impose a torque of $Q_2 = 100$ Nm in the joint between the first and the second arm of the multibody structure. We calculate the equilibrium position, and then we release the torque. During all the calculations, we treat the constraints as bilateral constraints. We analyse the results of time integration. The system integration starts from its non-equilibrium position. To obtain significant deformations of the beam (vital for the proposed testing of consistency of the constraint equations), we impose low stiffness of the beam elements. We demonstrate the calculated time evolution of the central point of the beam of the investigated system in Figure 4. We present the selected sketches of consecutive poses obtained by the system at different instants of time in Figure 5. We demonstrate the joined plot of two of them in Figure 3b, to simplify the comparison of the evolution of the pose.

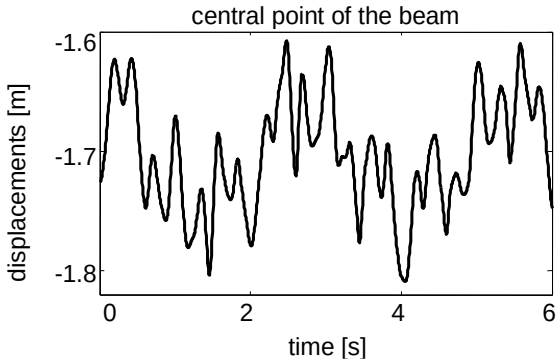

Figure 4. Time evolution of the investigated system: displacements of the central point of the investigated beam.

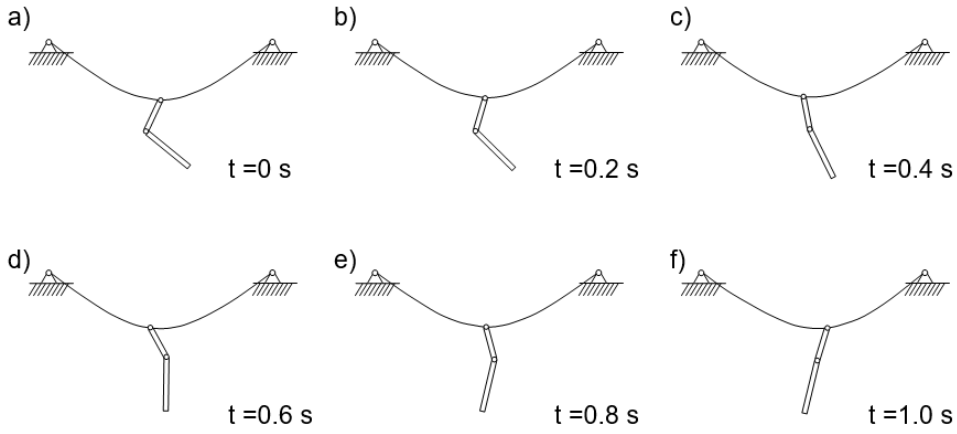

Figure 5. Time evolution of the investigated system: sketches of subsequent poses obtained by the system at different instants of time: initial position of $t = 0$ s (**a**); $t = 0.2$ s (**b**); $t = 0.4$ s (**c**); $t = 0.6$ s (**d**); $t = 0.8$ s (**e**); and $t = 1$ s (**f**).

9. Conclusions and Perspectives

Focusing on the obtained results, the proposed methodology, based on multibody and finite element modeling, can be successfully employed in contact analyses. Thanks to the proposed constraint formulae, the finite elements model and the sliding pendulum remain in permanent contact (bilateral). As we can see, we can express the investigated frictionless contact as a set of holonomic/scleronomic constraint equations. Additionally, we can successfully employ the coordinate partitioning technique to eliminate dependent coordinates and the Lagrange multipliers. The presented structure of the used equations convinced us that we could extend the above methodology to more complex systems, i.e., we can also effectively use the proposed procedure in the cases of models of contacts present between more complex mechanisms and more complex finite elements models.

We have to point out certain limitations in the applicability of the proposed procedure. Many authors of contemporary commercially accessible algorithms/programs design them with the black-box philosophy. Access to details of the used functions is limited. There is no access to internal modifications. Therefore, the proposed equations may be challenging in applicability, mainly because of a lack of detailed information about the applied commercial algorithms.

In future-coming investigations, we intend to extend the model with the friction phenomena and investigate the impacts at the contact point of the unilateral model of contacts (in both factionless and fictional contact cases). Non-punctual types of connections are in the scope of future investigations. We intend to investigate aspects connected with potentially overactuated configurations. We intend to propose methods for estimating the driving torques occurring in these configurations. We shall present the results of the optimization of these torques. We intend to suggest three-dimensional versions of these models. A complete model of the brachiation robot should be investigated numerically and in physical experiments done on material models.

Funding: This research received no external funding.

Institutional Review Board Statement: Not applicable.

Informed Consent Statement: Not applicable.

Data Availability Statement: Not applicable. All related data presented in this article.

Conflicts of Interest: The author declares no conflict of interest.

References

1. Allotta, B.; Pugi, L.; Bartolini, F. Design and development of a railway pantograph with a wire-pulley transmission system. In Proceedings of the ECCOMAS Thematic Conference in Multibody Dynamics, Milan, Italy, 25–28 June 2007.
2. Ambrosio, J.; Pombo, J.; Pereira, M.; Antunes, P.; Mosca, A. A Computational procedure for the dynamic analysis of the Catenary-pantograph interaction in High-speed trains. *J. Theor. Appl. Mech.* **2012**, *50*, 681–699.
3. Antuanes, P.; Ambrosio, J.; Pombo, J.; Facchinetti, A. A new methodology to study the pantograph-catenary dynamics in curved railway tracks. *Veh. Syst. Dyn.* **2020**, *58*, 425–452. [CrossRef]
4. Yang, C.J.; Zhang, W.H.; Zhang, J.; Mei, G.M.; Zhou, N.; Ren, G.X. Static form-finding analysis of a railway catenary using a dynamic equilibrium method based on flexible multibody system formulation with absolute nodal coordinates and controls. *Multibody Syst. Dyn.* **2017**, *39*, 221–247. [CrossRef]
5. Bauchau, O.A.; Bottasso, C.L. Contact Conditions for Cylindrical, Prismatic, and Screw Joints in Flexible Multibody Systems. *Multibody Syst. Dyn.* **2001**, *5*, 251–278. [CrossRef]
6. Qian, Z.; Zhang, D.; Jin, C. A regularized approach for frictional impact dynamics of flexible multi-link manipulator arms considering the dynamic stiffening effect. *Multibody Syst. Dyn.* **2018**, *43*, 229–255. [CrossRef]
7. Tang, L.; Liu, J. Frictional contact analysis of sliding joints with clearances between flexible beams and rigid holes in flexible multibody systems. *Multibody Syst. Dyn.* **2020**, *49*, 155–179. [CrossRef]
8. Shabana, A.A.; Ganito, F.M.; Brown, M.A. Integrations of finite element and multibody system algorithms for analysis of human body motion. *Procedia IUTAM* **2011**, *2*, 233–240. [CrossRef]
9. Bei, Y.; Fregly, B. Multibody dynamics simulation of the knee contact mechanics. *J. Med. Eng. Phys.* **2004**, *26*, 777–789. [CrossRef] [PubMed]
10. Schwab, A.L.; Meijaard, J.P. Two Special Finite Elements for Modeling Rolling Contact in a Multibody Environment. In Proceedings of the ACMD'02, The First Asian Conference on Multibody Dynamics 2002, Iwaki, Japan, 31 July –2 August 2002.
11. Antunes, P.; Magalhaes, H.; Ambrósio, J.; Pombo, J.; Costa, J. A co-simulation approach to the wheel–rail contact with flexible railway track. *Multibody Syst. Dyn.* **2019**, *45*, 245–272. [CrossRef]
12. Andreuchetti, S.; Oliveira, V.; Fukuda, T. A Survey on Brachiation Robots: An Energy-Based Review. *Robotica* **2021**, *39*, 1588–1600. [CrossRef]
13. Davies, E.; Garlow, A.; Farzan, S.; Rogers, J.; Hu, A.-P. Tarzan: Design, Prototyping, and Testing of a Wire-Borne Brachiating Robot. In Proceedings of the 2018 IEEE/RSJ International Conference on Intelligent Robots and Systems (IROS), Madrid, Spain, 1–5 October 2018; pp. 7609–7614. [CrossRef]
14. Lin, C.-Y.; Tian, Y.-J. Design of Transverse Brachiation Robot and Motion Control System for Locomotion between Ledges at Different Elevations. *Sensors* **2022**, *22*, 4031. [CrossRef] [PubMed]
15. Lo, A.K.-Y.; Yang, Y.-H.; Lin, T.-C.; Chu, C.-W.; Lin, P.-C. Model-Based Design and Evaluation of a Brachiating Monkey Robot with an Active Waist. *Appl. Sci.* **2017**, *7*, 947. [CrossRef]
16. Li, Y.; Zuo, M.-J.; Lin, J.; Liu, J. Fault detection method for railway wheel flat using an adaptive multiscale morphological filter. *Mech. Syst. Signal Process.* **2017**, *84*, 642–658. [CrossRef]
17. Li, Y.; Zhang, X.; Chen, Z.; Yang, Y.; Geng, C.; Zuo, M.-J. Time-frequency ridge estimation: An effective tool for gear and bearing fault diagnosis at time-varying speeds. *Mech. Syst. Signal Process.* **2023**, *189*, 110108. [CrossRef]
18. Skrinjar, L.; Slavic, J.; Boltezar, M. A review of continuous contact-force models in multibody dynamics. *Int. J. Mech. Sci.* **2018**, *145*, 171–187. [CrossRef]
19. Atanasovska, I. Multi-body contact in non-linear dynamics of real mechanical systems. *Procedia Eng.* **2017**, *199*, 510–515. [CrossRef]
20. Cavalieri, F.J.; Cardona, A.; Fachinotti, V.D.; Risso, J. A finite element formulation for Nonlinear 3D Contact Problem. *Mec. Comput.* **2007**, *26*, 1357–1372.
21. Seo, J.H.; Sugiyama, H.; Shabana, A.A. Three-Dimensional Large Deformation Analysis of the Multibody Pantograph/Catenary Systems. *Nonlinear Dyn.* **2005**, *42*, 199–215. [CrossRef]
22. Seo, J.H.; Kim, S.W.; Jung, I.H.; Park, T.W.; Mok, J.Y.; Kim, Y.G.; Chai, J.B. Dynamic Analysis of a pantograph-Catenary System Using Absolute Nodal Coordinates. *Veh. Syst. Dyn.* **2006**, *44*, 615–630. [CrossRef]
23. Kim, J.-G.; Han, J.-B.; Lee, H.; Kim, S.-S. Flexible multibody dynamics using coordinate reduction improved by dynamic correction. *Multibody Syst. Dyn.* **2018**, *42*, 411–429. [CrossRef]
24. Lipinski, K. Multibody System in a Contact with a Model Composed of Finite Elements. In Proceedings of the ECCOMAS Thematic Conference in Multibody Dynamics, Warsaw, Poland, 29 June–2 July 2009.
25. Lipinski, K. Constraints equations, a numerical method to connect a multibody model with a finite element model when a planar mechanism slides with a friction on a beam. In Proceedings of the CMM-2011—Computer Methods in Mechanics, Warsaw, Poland, 9–12 May 2011.
26. Lipinski, K. *Multibody Systems with Unilateral Constraints in Application to Modelling of Complex Mechanical Systems*; Seria Monografie, 123; Wydawnictwo Politechniki Gdańskiej: Gdańsk, Poland, 2012. (In Polish)
27. Fisette, P.; Lipinski, K.; Samin, J.C. Modelling for the Simulation Control and Optimization of Multibody System. In *Advances in Multibody Systems and Mechatronics*; contributions dedicated to Prof. Manfred Hiller on the occasion of his sixtieth birthday; Duisburg, Germany, September 25, 1999; Inst. für Mechanik und Getriebelehre: Graz, Austria, 1999; pp. 139–174.

28. Fisette, P.; Samin, J.C. *Symbolic Modeling of Multibody System*; Kluwer Academic Publishers: Dordrecht, The Netherlands, 2003.
29. Gawroński, W.; Kruszewski, J.; Ostachowicz, W.; Tarnowski, J.; Wittbrodt, E. *Metoda Elementów Skończonych w Dynamice Konstrukcji*; Arkady: Warszawa, Poland, 1984. (In Polish)
30. Kruszewski, J.; Wittbrodt, E.; Walczyk, Z. *Drgania Układów Mechanicznych w Ujęciu Komputerowym, Tom 2*; WNT: Warszawa, Poland, 1993. (In Polish)
31. Zienkiewicz, O.C.; Taylor, R.L. *The Finite Element Method*, 5th, ed.; Volume 1: The Basis; Butterworth-Heinemann: Oxford, UK, 2000.
32. Haug, E.J.; Yen, J. Generalized Coordinate Partitioning Method for Numerical Integration. In *Real-Time Integration Methods for Mechanical System Simulation*; NATO ASI Series; Springer: Berlin/Heidelberg, Germany, 1990; Volume 69, pp. 97–114.
33. Matlab. Available online: https://www.mathworks.com/products/matlab.html (accessed on 15 January 2023).